



# Tailoring assemblies of plasmonic silver/gold and zinc–gallium layered double hydroxides for photocatalytic conversion of carbon dioxide using UV–visible light



Shogo Kawamura<sup>a</sup>, Magda C. Puscasu<sup>b</sup>, Yusuke Yoshida<sup>a</sup>, Yasuo Izumi<sup>a,\*</sup>, Gabriela Carja<sup>b,\*\*</sup>

<sup>a</sup> Department of Chemistry, Graduate School of Science, Chiba University, Yayoi 1-33, Inage-ku, Chiba 263-8522, Japan

<sup>b</sup> Department of Chemical Engineering, Faculty of Chemical Engineering and Environmental Protection, Technical University, "Gh. Asachi" of Iasi, Bd. Mangeron No. 71, Iasi 700554, Romania

## ARTICLE INFO

### Article history:

Received 17 September 2014

Received in revised form

19 December 2014

Accepted 22 December 2014

Available online 2 January 2015

### Keywords:

CO<sub>2</sub> photoreduction

Layered double hydroxide

Silver

Gold

Surface plasmon resonance

## ABSTRACT

In the search for novel efficient photocatalysts for the conversion of CO<sub>2</sub> into fuels, plasmonic photocatalysts based on the self-assemblies of silver or gold nanoparticles with [Zn<sub>3</sub>Ga(OH)<sub>6</sub>]<sub>2</sub>CO<sub>3</sub>·mH<sub>2</sub>O layered double hydroxide (Zn<sub>3</sub>Ga|CO<sub>3</sub> LDH) were prepared and tested for the photoreduction of CO<sub>2</sub> by H<sub>2</sub> under irradiation with UV–visible light. Ag and Au nanoparticles were obtained directly on the LDHs via the ion-exchange method or the reconstruction method of the LDHs. The catalysts exhibited intense surface plasmon resonance (SPR) effect at 411 and 555 nm attributable to Ag and Au nanoparticles, respectively. The rate of CO<sub>2</sub> photoreduction on Ag/Zn<sub>3</sub>Ga|CO<sub>3</sub> increased by a factor of 1.69 than that of Zn<sub>3</sub>Ga|CO<sub>3</sub> while the methanol selectivity also increased from 39 to 54 mol%. On Au/Zn<sub>3</sub>Ga|CO<sub>3</sub>, the reduction rate of CO<sub>2</sub> was 1.78 times higher than on Zn<sub>3</sub>Ga|CO<sub>3</sub> LDH whereas the methanol selectivity decreased from 39 to 13 mol%. Electron microscopy and UV–visible and X-ray spectroscopy detected particular interactions of the cationic layers of Zn<sub>3</sub>Ga|CO<sub>3</sub> with Ag and Au nanoparticles. Results show that for Ag/Zn<sub>3</sub>Ga|CO<sub>3</sub> catalysts, CO<sub>2</sub> photoreduction by H<sub>2</sub> under visible light was promoted by the SPR effect of Ag nanoparticles while for Au/Zn<sub>3</sub>Ga|CO<sub>3</sub> catalysts Au nanoparticles might act as electron-trapping active sites.

© 2014 Elsevier B.V. All rights reserved.

## 1. Introduction

The increasing concentration of CO<sub>2</sub> in the atmosphere, as a result of the combustion of the carbon-based fuels, is predicted to result in unacceptable changes in the Earth's climate [1,2]. The photoreduction of CO<sub>2</sub> to fuels using light energy can contribute simultaneously to reduction of the major greenhouse gas and the development of sustainable energy. A key technological target to reach efficient photoconversion of CO<sub>2</sub> to fuels (i.e. artificial photosynthesis) is to develop an efficient and robust photocatalyst [3]. An important factor limiting the conversion efficiency of almost every active photocatalyst is the high rate of charge carrier recombination. Recently, Ingram and Linic [4] demonstrated that the recombination problem was significantly alleviated by assembling plasmonic nanoparticles and semiconductor supports. Moreover, it

has been recently reported that in plasmonic nanoparticles/support co-catalytic systems the photo-responsive features of the metal nanoparticles that manifest the surface plasmon resonance (SPR) effect are able to tune and assist the photocatalytic properties of the support. The particular features of the plasmonic nanostructures at the support interface might reduce the charge carrier recombination rate, and thereby enhance the visible-light-induced photocatalytic activities.

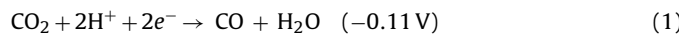
Layered double hydroxides (LDHs) or hydrotalcite-like materials are layered porous matrices belonging to the class of anionic clay (cationic layers intercalating anions) with many actual and potential applications in catalysis [5]. Recently, García group introduced a novel concept of Ti, Ce, or Cr-doped semiconductors based on Zn-containing LDHs [6]. LDHs can be defined by a versatile elemental composition and the ratio, and have basic properties and a high adsorption capacity for CO<sub>2</sub> [7]. LDH photocatalysts comprising Zn and Ga have been reported, in our previous work, to convert CO<sub>2</sub> into methanol or CO using H<sub>2</sub> [8–10]. The photocatalytic reduction of CO<sub>2</sub> using water and LDHs [11] and the combination of photooxidation catalyst and LDHs were also reported [12]. However, the

\* Corresponding author. Tel.: +81 43 290 3696; fax: +81 43 290 2783.

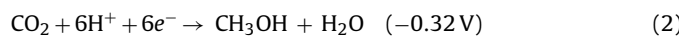
\*\* Corresponding author. Tel.: +40 232 201231; fax: +40 232 201231.

E-mail addresses: [yizumi@faculty.chiba-u.jp](mailto:yizumi@faculty.chiba-u.jp) (Y. Izumi), [carja@uaic.ro](mailto:carja@uaic.ro) (G. Carja).

band gap of these LDHs, e.g. 5.6 eV for  $[Zn_3Ga(OH)_8]_2CO_3 \cdot mH_2O$ , corresponded to ultraviolet (UV) region and accordingly these LDHs were primarily responsive to UV light [10]. The relatively wide band gap was advantageous to set the conduction band (CB) minimum enough negative for these LDHs compared to the reduction reaction potentials of



and



versus standard hydrogen electrode (SHE) [10]. It is essential to utilize visible light, 97% of the spectrum of solar radiation [13], while utilizing the enough negative potential of CB minimum.

In this work,  $[Zn_3Ga(OH)_8]_2CO_3 \cdot mH_2O$  was combined with a sensitizer of silver or gold nanoparticles that are responsive to visible light. For Ag nanoparticles dispersed in liquid, the corresponded SPR peak progressively shifted from 405 nm to 510 nm as the Ag particles grows from 10 nm to 100 nm [14]. Further, the SPR peak progressively shifted from 515 nm to 572 nm as the Au nanoparticles grows from 5 nm to 100 nm [15]. The hybridization of SPR of 100 nm of Ag cube and silicon nitride substrate at the interface was visualized by electron energy loss spectroscopy in a monochromated scanning transmission electron microscopy (TEM) [16]. Plasmon-induced excited electron injection from nanoparticles, e.g. Ag and Au, to semiconductors, e.g.  $TiO_2$ , exceeding the Schottky barrier, has been reported [17–20]. Mean 7 nm of Ag nanoparticles were combined with a LDH material of  $[Zn_2Al(OH)_6]_2CO_3 \cdot mH_2O$  by the reaction of aqueous solution of  $Ag^+$  salt with the LDH powder freshly calcined at 823 K [21] while mean 2.9 and 3.4 nm of Au nanoparticles were combined with a LDH of  $[Zn_2Al(OH)_6]_2CO_3 \cdot mH_2O$  and  $[Zn_2Al_{0.7}Ce_{0.3}(OH)_6]_2CO_3 \cdot mH_2O$  by the reaction of aqueous solution of  $Au^{3+}$  with the LDH calcined at 823 K [22]. Based on these procedures, the anionic clay was transformed into metal oxides upon calcination at 823 K. The layered structure LDH was then reconstructed when the calcined LDH at 823 K was introduced into the aqueous solutions of silver or gold salts [21,22]. In this work, assemblies of Ag and Au nanoparticles and  $[Zn_3Ga(OH)_8]_2CO_3 \cdot mH_2O$  were obtained via ion-exchange method at 290 K or via the structural reconstruction of the LDHs in the specific aqueous solutions of Ag or Au. It is noteworthy that Ag and Au nanoparticles were obtained directly on the LDH platelets and no organic products were used during the preparation of Ag/LDH and Au/LDH assemblies via the reconstruction method. We present here the performances of Ag/ $[Zn_3Ga(OH)_8]_2CO_3 \cdot mH_2O$  and Au/ $[Zn_3Ga(OH)_8]_2CO_3 \cdot mH_2O$  for the photoconversion of  $CO_2$  using  $H_2$  and UV and visible light.

## 2. Experimental

### 2.1. Sample synthesis

LDH compound of  $[Zn_3Ga(OH)_8]_2CO_3 \cdot mH_2O$  was synthesized using a reported procedure from metal nitrates,  $Na_2CO_3$ , and  $NaOH$  in aqueous solutions controlled at pH 8 [10]. This compound is abbreviated as  $Zn_3Ga|CO_3$ .

For the ion exchange method, we followed the procedure presented in Ref. [23]. Firstly, 0.50 g of  $Zn_3Ga|CO_3$  powder was immersed in an aqueous solution of  $AgNO_3$  (>99.8%, Wako Pure Chemical; 0.050 M, 10 mL) in a flask and refluxed at 353 or 373 K for 15 min, magnetically stirred at 900 rotations per minute (rpm). The yellow precipitates that were obtained were filtered using a polytetrafluoroethylene-based membrane filter (Omnipore JGWP04700, Millipore) with a pore size of 0.2  $\mu\text{m}$  and washed well with deionized water ( $<0.06\text{ }\mu\text{S cm}^{-1}$ ; total 250 mL). The precipitates that were obtained were dried in oven at 333 K for 24 h.

These yellow samples were denoted as  $Ag/Zn_3Ga|CO_3$ -IE353-15 and  $Ag/Zn_3Ga|CO_3$ -IE373-15, respectively.

The sample denoted as  $Ag/Zn_3Ga|CO_3$ -IE373-180 was obtained via a similar procedure to that described for  $Ag/Zn_3Ga|CO_3$ -IE373-15, however, in this case the time of reflux was extended up to 3 h. A gray precipitate was obtained.

Next, Ag nanoparticles were obtained and organized with  $Zn_3Ga|CO_3$  using the LDH reconstruction method [21]. 1.2 g of  $Zn_3Ga|CO_3$  powder was calcined in an oven at 773 K for 8 h. After the calcination, hot powder derived from  $Zn_3Ga|CO_3$  was directly added into 200 mL aqueous solution of  $Ag(I)$  acetate (>99.9%, Alfa Aesar; 0.10 g) stirring at a rate of 900 rpm. The pH of the solution was adjusted to 8.0 by the addition of  $NaOH$  aqueous solution (0.10 M). The reaction mixture was stirred at the rate of 900 rpm and 290 K for 20 min and then at the rate of 150 rpm and 313 K for 5 h. Then, the precipitate was centrifuged at the rate of 10,000 rpm and dried in an oven at 353 K for 1 h. The obtained light brown sample was denoted as  $Ag/Zn_3Ga|CO_3$ -reconst.

$Au/Zn_3Ga|CO_3$  was obtained by the ion exchange method followed by the liquid phase reduction according to the similar procedure reported in Ref. [24]. 0.022 g of hydrochloroauric acid tetrahydrate (>99.9%, Alfa Aesar) was dissolved in 10 mL of deionized water. 0.60 g of  $Zn_3Ga|CO_3$  was added to the aqueous solution and the mixture was stirred at 290 K for 12 h. The precipitate was filtered using a JGWP04700 filter, washed with deionized water (total 250 mL), and dried. Obtained powder was added to 5 mL of dehydrated toluene (>99.5%, Wako Pure Chemical) and 0.0063 g of  $NaBH_4$  (>95%, Wako Pure Chemical) was added to the suspension. After stirring for 10 min, 1.5 mL of ethanol was added and the mixture was stirred at 290 K for 6 h. The obtained purple precipitate was collected by filtration using a JGWP04700 filter, washed with deionized water and ethanol (total 250 mL for each), and dried under vacuum at 290 K for 24 h. This sample was denoted as  $Au/Zn_3Ga|CO_3$ -IE.

$Au/Zn_3Ga|CO_3$ -reconst: in this case, the assembly of Au nanoparticles with  $Zn_3Ga|CO_3$  was obtained using the structural reconstruction of LDH in the aqueous solutions containing  $Au^{3+}$  [22]. Hence, 1.20 g  $Zn_3Ga|CO_3$  powder was calcined in an oven at 773 K for 8 h. The resulted hot calcined powder was directly added into 200 mL aqueous solution of  $Au(III)$  acetate (>99.9%, Alfa Aesar; 0.10 g) stirring at a rate of 900 rpm. The pH of the solution was adjusted to 8.0 by the addition of  $NaOH$  aqueous solution (0.1 M). The reaction mixture was stirred at the rate of 900 rpm and 290 K for 20 min and then at the rate of 150 rpm and 313 K for 5 h. Then, the precipitate was centrifuged at the rate of 10,000 rpm and dried in an oven at 353 K for 1 h. The color of this catalyst was light purple.

### 2.2. Characterization

Optical spectroscopic measurements were performed using a UV-visible spectrophotometer (Model V-650, JASCO) using  $D_2$  and halogen lamps for wavelengths between 200 and 340 nm and between 340 and 800 nm, respectively. An integrating sphere (Model ISV-469, JASCO) was used for the diffuse reflectance (DR) measurements. The samples were set in contact with the quartz window glass in a gas-tight DR cell. The measurements were performed at 290 K within the wavelength range 200–800 nm using 70 mg of sample. DR spectra were converted to absorption spectra on the basis of the Kubelka–Munk equation [9,10]. The bandgap ( $E_g$ ) value was evaluated on the basis of either simple extrapolation of the absorption edge or the fit to the Davis–Mott equation,

$$\alpha \propto h\nu \propto (h\nu - E_g)^n \quad (3)$$

in which  $\alpha$ ,  $h$ , and  $\nu$  are the absorption coefficient, Planck's constant, and the frequency of light, respectively, and  $n$  is 1/2, 3/2, 2, and

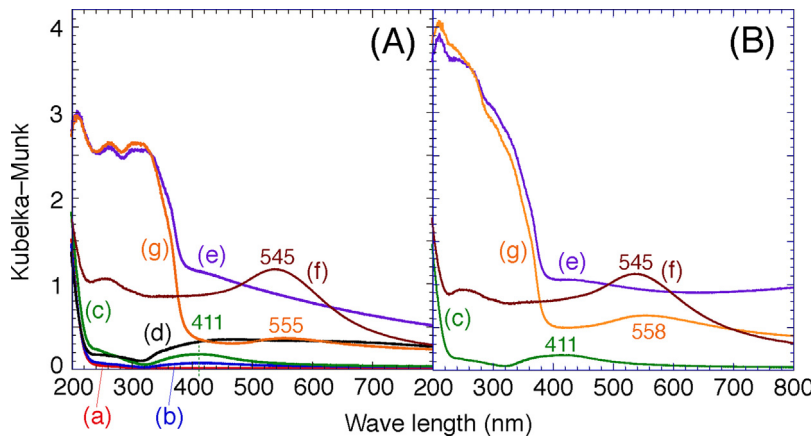


**Fig. 1.** UV-visible absorption spectrum for as-synthesized samples (A) of  $\text{Zn}_3\text{Ga}|\text{CO}_3$  (a),  $\text{Ag}/\text{Zn}_3\text{Ga}|\text{CO}_3$ -IE353-15 (b),  $\text{Ag}/\text{Zn}_3\text{Ga}|\text{CO}_3$ -IE373-15 (c),  $\text{Ag}/\text{Zn}_3\text{Ga}|\text{CO}_3$ -IE373-180 (d),  $\text{Ag}/\text{Zn}_3\text{Ga}|\text{CO}_3$ -reconst (e),  $\text{Au}/\text{Zn}_3\text{Ga}|\text{CO}_3$ -IE (f), and  $\text{Au}/\text{Zn}_3\text{Ga}|\text{CO}_3$ -reconst (g) and samples after photocatalytic tests for 5 h (B) of  $\text{Ag}/\text{Zn}_3\text{Ga}|\text{CO}_3$ -IE373-15 (c),  $\text{Ag}/\text{Zn}_3\text{Ga}|\text{CO}_3$ -reconst (e),  $\text{Au}/\text{Zn}_3\text{Ga}|\text{CO}_3$ -IE (f), and  $\text{Au}/\text{Zn}_3\text{Ga}|\text{CO}_3$ -reconst (g).

3 for allowed direct, forbidden direct, allowed indirect, and forbidden indirect electronic transitions, respectively [25]. The value of  $n$  was also estimated by the fit to Eq. (4).

$$\ln(\alpha \times h\nu) \propto n \ln(h\nu - E_g) \quad (4)$$

X-ray diffraction (XRD) pattern was observed using a D8 ADVANCE diffractometer (Bruker) at the Center for Analytical Instrumentation, Chiba University, at a Bragg angle of  $2\theta_B = 3\text{--}60^\circ$  with a scan step of  $0.01^\circ$  and a scan rate of 5 s per step. The measurements were performed at 40 kV and 40 mA using Cu K $\alpha$  emission and a nickel filter.

Scanning electron microscopy (SEM) measurements were performed using JEOL Model JSM6510A at the Center for Analytical Instrumentation. The samples were mounted on a conducting carbon tape and coated with gold. The electron accelerating voltage was 15 kV and the magnification was between 20,000 and 50,000 times.

High-resolution (HR)-TEM images were observed using transmission electron microscope (Model H-7650, Hitachi) operating at 100 kV. Tungsten filament was used in the electron gun and the samples were mounted on a conducting carbon with Cu grid mesh (150 mesh per inch) and the magnification was between 60,000 and 200,000 times.

Ag K-edge and Au L<sub>3</sub>-edge X-ray absorption fine structure (XAFS) spectra were measured at 290 K in transmission mode in the Photon Factory Advanced Ring at the High Energy Accelerator Research Organization (Tsukuba) on beamline NW10A. The storage ring energy was 6.5 GeV and the ring current was 46.6–36.1 mA. A Si (3 1 1) double-crystal monochromator and platinum-coated focusing cylindrical mirror were inserted into the X-ray beam path. The X-ray intensity was maintained at 65% of the maximum flux using a piezo translator set to the crystal. The slit opening size was 1 mm (vertical)  $\times$  2 mm (horizontal) in front of the ionization chamber. The Ag K and Au L<sub>3</sub>-edge absorption energy was calibrated to 25,516.5 eV and 11,921.2 eV for the spectrum of Ag and Au metal foil, respectively [26].

The XAFS data were analyzed using an XDAP package [27]. The pre-edge background was approximated by a modified Victoreen function  $(C_2/E^2) + (C_1/E) + C_0$ . The background of the post-edge oscillation was approximated by a smoothing spline function and

calculated by an equation for the number of data points, where  $k$  is the wavenumber of photoelectrons.

$$\sum_{i=1}^{\text{Data\_Points}} \frac{(\mu x_i - BG_i)^2}{\exp(-0.075k_i^2)} \leq \text{smoothing factor} \quad (5)$$

Multiple-shell curve-fit analyses were performed for the Fourier-filtered  $k^3$ -weighted extended XAFS (EXAFS) data in  $k$ - and  $R$ -space using empirical amplitude extracted from the EXAFS data for Ag metal foil,  $\text{Ag}_2\text{O}$  powder, and Au metal foil [28]. The interatomic distance ( $R$ ) and its associated coordination number ( $N$ ) for the Ag–Ag, Ag–O, and Au–Au pairs were set to 0.288 9 nm with the  $N$  value of 12 [29], 0.204 4 nm with the  $N$  value of 2 [30], and 0.288 4 nm with the  $N$  value of 12 [31], respectively. The many-body reduction factor  $S_0^{-2}$  was assumed to be equal for both the sample and the reference.

### 2.3. Photocatalytic conversion tests for $\text{CO}_2$

As-synthesized and preheated samples of LDHs were tested for the photocatalytic conversion of  $\text{CO}_2$  [9,10]. The tests were conducted in a closed circulating system (171 mL) equipped with a photoreaction quartz cell that had a flat bottom ( $23.8 \text{ cm}^2$ ). 100 mg of the LDH catalyst was uniformly spread in the photoreaction cell and was evacuated by rotary and diffusion pumps ( $10^{-6} \text{ Pa}$ ) at 290 K for 2 h until the desorbed gas was detected by an online gas chromatograph (GC). 2.3 kPa of  $\text{CO}_2$  (0.177 mmol) and 21.7 kPa of  $\text{H}_2$  (1.67 mmol) were introduced to both intact and pretreated LDH photocatalysts and were allowed to circulate for 30 min in contact with the catalyst to attain sorption equilibrium before irradiation.

The photocatalyst was then irradiated with UV-visible light from the 500-W xenon arc lamp (Ushio, Model UI-502Q) from downward through the flat bottom of the quartz reactor for 5 h. The distance between the bottom of the reactor and the lamp house exit window was set to 20 mm. The light intensity was  $42 \text{ mW cm}^{-2}$  at the center of the sample cell and  $28 \text{ mW cm}^{-2}$  at the periphery of the bottom plate of the sample cell. The temperature was within the range 305–313 K at the catalyst position during the illumination for 5 h. As comparison, the photocatalyst was irradiated with visible light using a UV-cut filter that passes light ( $\lambda > 420 \text{ nm}$ ) (L42, Kenko) between the light exit of UI-502Q and photocatalyst. Products and reactants were analyzed using packed columns of molecular sieve 13X-S and polyethylene glycol (PEG-6000) supported on Flusin P

**Table 1**

Physicochemical characterization of  $\text{Zn}_3\text{Ga}|\text{CO}_3$  LDHs ensembled with Ag or Au nanoparticles.

Photocatalyst	Color	Plasmon peak (nm)	Ag/Au particle size (nm)		$E_g$ (eV)	$n$ [Eq. (4)]	Interlattice distance (nm)
			TEM <sup>b</sup>	EXAFS			
<i>(A) As fresh</i>							
$\text{Zn}_3\text{Ga} \text{CO}_3$	White	—	—	—	5.6	5.4 (3/2)	1.07
$\text{Ag}/\text{Zn}_3\text{Ga} \text{CO}_3\text{-IE353-15}$	Yellow	411	—	—	5.6	5.4 (3/2)	1.07
$\text{Ag}/\text{Zn}_3\text{Ga} \text{CO}_3\text{-IE373-15}$	Yellow	411	5.4–27	1.6	5.5	5.3 (3/2)	1.04
$\text{Ag}/\text{Zn}_3\text{Ga} \text{CO}_3\text{-IE373-180}$	Gray	(flat)	—	3.7	5.5	5.4 (3/2)	1.22
$\text{Ag}/\text{Zn}_3\text{Ga} \text{CO}_3\text{-reconst}^a$	Light brown	(flat)	—	3.6	3.1	3.1 (1/2)	0.71
$\text{Au}/\text{Zn}_3\text{Ga} \text{CO}_3\text{-IE}$	Purple	545	—	3.2	1.9	5.5 (3/2)	1.07
$\text{Au}/\text{Zn}_3\text{Ga} \text{CO}_3\text{-reconst}^a$	Light purple	555	—	2.6	3.0	3.1 (3/2, 2)	1.94
<i>(B) After photocatalytic test in <math>\text{CO}_2</math> (2.3 kPa) + <math>\text{H}_2</math> (21.7 kPa) for 5 h</i>							
$\text{Zn}_3\text{Ga} \text{CO}_3$	White	—	—	—	5.6	—	—
$\text{Ag}/\text{Zn}_3\text{Ga} \text{CO}_3\text{-IE353-15}$	Yellow	411	—	—	5.6	—	—
$\text{Ag}/\text{Zn}_3\text{Ga} \text{CO}_3\text{-IE373-15}$	Yellow	411	—	—	5.5	—	—
$\text{Ag}/\text{Zn}_3\text{Ga} \text{CO}_3\text{-IE373-180}$	Gray	(wide, flat)	—	—	5.5	—	—
$\text{Ag}/\text{Zn}_3\text{Ga} \text{CO}_3\text{-reconst}^a$	Gray	(wide, flat)	—	2.0	3.1	3.1 (1/2)	0.82
$\text{Au}/\text{Zn}_3\text{Ga} \text{CO}_3\text{-IE}$	Purple	545	—	—	5.4	5.0 (3/2)	0.94
$\text{Au}/\text{Zn}_3\text{Ga} \text{CO}_3\text{-reconst}^a$	Purple	555	—	1.7	3.0	3.0 (2)	2.01

<sup>a</sup> Preheated at 373 K for 30 min. The layered structure of all the samples in this study was stable at this condition.

<sup>b</sup> Most frequent particle size in histogram for HR-TEM images.

(GL Sciences) set in the online GC equipped with a thermal conductivity detector (Shimadzu, Model GC-8A).

### 3. Results

#### 3.1. Characterization of the Ag/LDH and Au/LDH assemblies

DR UV-visible spectra for as-synthesized Ag/LDHs and Au/LDHs composites are summarized in Fig. 1A. The absorption edge was in UV light region for all the samples. The absorption edge was extrapolated to give the  $E_g$  value of 5.6–5.1 eV for  $\text{Zn}_3\text{Ga}|\text{CO}_3$ ,  $\text{Ag}/\text{Zn}_3\text{Ga}|\text{CO}_3\text{-IE}$ , and  $\text{Au}/\text{Zn}_3\text{Ga}|\text{CO}_3\text{-IE}$ , and the  $E_g$  value of 3.1–3.0 eV for  $\text{Zn}_3\text{Ga}|\text{CO}_3$  reconstructed with Ag or Au (Table 1A). The former values were consistent with previous study for the LDHs [10], but the latter values should be affected by the impurity metal oxide phase(s) (see the XRD section below). If the spectra were fitted to Eq. (3), similar  $E_g$  values were given when the  $n$  value was 3/2 or 1/2 except for  $\text{Au}/\text{Zn}_3\text{Ga}|\text{CO}_3\text{-reconst}$  (Table 1A). Thus, the electronic transition could be a direct process from O 2p to metal 4s or 4p of Zn, Ga from  $\text{Zn}_3\text{Ga}|\text{CO}_3$  layers or impurity metal oxides except for  $\text{Au}/\text{Zn}_3\text{Ga}|\text{CO}_3\text{-reconst}$ .

In fact, when the data for the as-synthesized samples were fit to Eq. (4) using the  $E_g$  values obtained by the extrapolation of the absorption edge (Table 1A),  $n$  values of 0.71–1.22 were given suggesting a direct electronic transition process except for  $\text{Au}/\text{Zn}_3\text{Ga}|\text{CO}_3\text{-reconst}$  (Table 1). The  $n$  value for  $\text{Au}/\text{Zn}_3\text{Ga}|\text{CO}_3\text{-reconst}$  was significantly greater (1.94), suggesting allowed indirect electronic transition ( $n=2$ ) [25] modulated by the joining assembly of  $\text{Zn}_3\text{Ga}|\text{CO}_3$  and Au nanoparticles. This modulation implied specific photocatalytic role of Au (see Section 3.2).

No absorption appeared for  $\text{Zn}_3\text{Ga}|\text{CO}_3$  except for the absorption edge below 230 nm (Fig. 1A-a) [10]. In contrast,  $\text{Ag}/\text{Zn}_3\text{Ga}|\text{CO}_3\text{-IE353-15}$ ,  $\text{Ag}/\text{Zn}_3\text{Ga}|\text{CO}_3\text{-IE373-15}$ ,  $\text{Au}/\text{Zn}_3\text{Ga}|\text{CO}_3\text{-IE}$ , and  $\text{Au}/\text{Zn}_3\text{Ga}|\text{CO}_3\text{-reconst}$  absorbed light centered at 411, 411, 545, and 555 nm, respectively (Fig. 1A-b, c, f, g). A peak centered at 533–553 nm was reported for 2.9–3.4 nm of Au nanoparticles on LDH comprising Zn and Al and LDH comprising Zn, Al, and Ce [22].

The absorption for  $\text{Ag}/\text{Zn}_3\text{Ga}|\text{CO}_3\text{-IE373-180}$  and  $\text{Ag}/\text{Zn}_3\text{Ga}|\text{CO}_3\text{-reconst}$  ranged whole visible light region (Fig. 1A-d, e) rather than forming a peak, revealing the formation of large size Ag nanoparticles and/or a wider size distribution of Ag nanoparticles.

The UV-visible spectra of the catalysts were also measured after photocatalytic tests in  $\text{CO}_2$  (2.3 kPa) and  $\text{H}_2$  (21.7 kPa) for 5 h.

Negligible change was observed for  $\text{Ag}/\text{Zn}_3\text{Ga}|\text{CO}_3\text{-IE373-15}$  and  $\text{Au}/\text{Zn}_3\text{Ga}|\text{CO}_3\text{-IE}$  (Fig. 1A-c, f and B-c, f), demonstrating the stability of the catalysts during 5 h of irradiation under the reactants. On the contrary, the absorption increased in the range between 550 and 800 nm by at most 1.94 times for  $\text{Ag}/\text{Zn}_3\text{Ga}|\text{CO}_3\text{-reconst}$  (Fig. 1A-e, B-e) while the peak intensity at 555 nm of the as-synthesized sample (Fig. 1A-g) increased by 1.72 times after the photocatalytic test (558 nm; Fig. 1B-g) for  $\text{Au}/\text{Zn}_3\text{Ga}|\text{CO}_3\text{-reconst}$ .

Hence, Ag nanoparticles in  $\text{Ag}/\text{Zn}_3\text{Ga}|\text{CO}_3\text{-reconst}$  catalyst became larger in size due to the aggregation process. On the contrary, Au nanoparticles of  $\text{Au}/\text{Zn}_3\text{Ga}|\text{CO}_3\text{-reconst}$  preserved their size although their number increased due to the reduction of Au oxide nanoparticles and/or to the aggregation of the well-dispersed ionic  $\text{Au}^{3+}$  into metallic Au nanoparticles during the 5 h photocatalytic tests. It is noteworthy that the aggregation of Ag nanoparticles and the increase of the number of Au nanoparticle were consistent with the change of the color of these photocatalysts from the light brown to gray and from light purple to purple, respectively, after the photocatalytic test for 5 h (Table 1A and B).

The XRD pattern of  $\text{Zn}_3\text{Ga}|\text{CO}_3$ ,  $\text{Ag}/\text{Zn}_3\text{Ga}|\text{CO}_3\text{-IE373-15}$ ,  $\text{Ag}/\text{Zn}_3\text{Ga}|\text{CO}_3\text{-reconst}$ ,  $\text{Au}/\text{Zn}_3\text{Ga}|\text{CO}_3\text{-IE}$ , and  $\text{Au}/\text{Zn}_3\text{Ga}|\text{CO}_3\text{-reconst}$  are depicted in Fig. 2. The diffraction peaks common at  $2\theta_B = 11.7^\circ, 23.5^\circ, 33.5^\circ, 34.2^\circ, 37.0^\circ, 38.9^\circ, 43.7^\circ, 46.5^\circ, 52.7^\circ, 56.1^\circ$ , and  $59.4^\circ$  were assigned to 003, 006, 009, 012, 104, 107, 111, 110, 108, 015, 014, 009, 012, 006, 003, and 003, respectively. The peaks marked with asterisks (\*) and plus (+) signs were assigned to  $\beta\text{-Ga}_2\text{O}_3$  and  $\alpha\text{-GaO(OH)}$ , respectively. The peaks marked with inverted triangles (▽) and triangles (△) were assigned to  $\text{ZnO}$  and  $\text{Zn(OH)}_2$ , respectively.

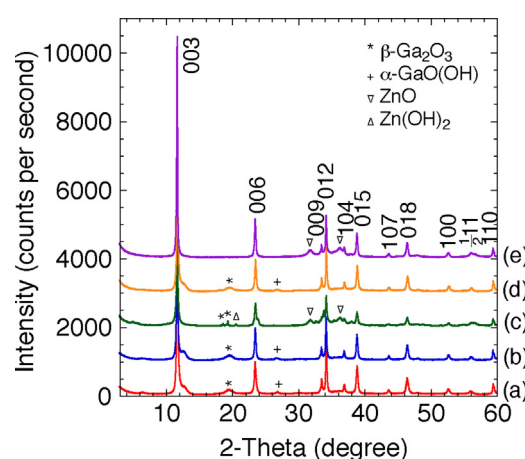


Fig. 2. XRD pattern of  $\text{Zn}_3\text{Ga}|\text{CO}_3$  (a),  $\text{Ag}/\text{Zn}_3\text{Ga}|\text{CO}_3\text{-IE373-15}$  (b),  $\text{Ag}/\text{Zn}_3\text{Ga}|\text{CO}_3\text{-reconst}$  (c),  $\text{Au}/\text{Zn}_3\text{Ga}|\text{CO}_3\text{-IE}$  (d), and  $\text{Au}/\text{Zn}_3\text{Ga}|\text{CO}_3\text{-reconst}$  (e).

015, 107, 018, 100,  $\frac{1}{2}11$  ( $=01\bar{1}1$ ), and 110 diffraction for the regular layered structure of LDH, respectively. The interlayer interval value was evaluated to 0.752–0.754 nm on the basis of the 003 diffraction angle and negligibly changed combined with Ag or Au (Table 1). This indicates that nanosized Ag and Au formed via the ion exchange and via the LDH reconstruction were exclusively adsorbed on the external surface of LDHs.

For  $Zn_3Ga|CO_3$ ,  $Ag/Zn_3Ga|CO_3$ -IE373-15, and  $Au/Zn_3Ga|CO_3$ -IE samples, weak peaks derived from  $\beta$ - $Ga_2O_3$  201 lattice and  $\alpha$ - $GaO(OH)$  110 lattice [32] can be also observed at  $2\theta_B = 19.6^\circ$  and  $26.8$ – $26.9^\circ$ , respectively (Fig. 2a, b, d). For the  $Ag/Zn_3Ga|CO_3$ -reconst and  $Au/Zn_3Ga|CO_3$ -reconst samples, peaks derived from  $ZnO$  100 and 101 reflection appeared at  $2\theta_B = 31.8^\circ$  and  $36.3^\circ$  respectively [33]. As the peaks due to  $ZnO$  impurity did not appear for  $Zn_3Ga|CO_3$ ,  $Ag/Zn_3Ga|CO_3$ -IE373-15, and  $Au/Zn_3Ga|CO_3$ -IE, minor amount of  $ZnO$  remained when once calcined oxide from LDH was reconstructed in the specific  $Ag^+$  or  $Au^{3+}$  aqueous solutions. For the  $Ag/Zn_3Ga|CO_3$ -reconst sample, weak peaks derived from  $\beta$ - $Ga_2O_3$  020 and 201 lattices [32] and  $Zn(OH)_2$  110 lattice [34,35] were observed at  $2\theta_B = 18.7^\circ$ ,  $19.4$ , and  $20.7^\circ$ , respectively.

The morphology of the LDH composites was studied by SEM. Fig. 3 shows the SEM image of  $Ag/Zn_3Ga|CO_3$ -IE373-15. Flat platelets with the lateral size between 200 and 700 nm and the thickness between 20 and 50 nm, that are typical for the layered structure of LDH, were clearly observed. According to SEM analysis, a similar morphology of the platelets for LDH crystallites was observed for all the catalysts. On the other hand, the Ag nanoparticles were not observed by the spacial resolution of SEM (Fig. 3). Thus, we further observed the HR-TEM images for studying the composites of the LDHs with Ag or Au nanoparticles.

$Ag$  nanoparticles (5.4–27 nm) originating from ion-exchanged  $Ag^+$  are presented in HR-TEM image for  $Ag/Zn_3Ga|CO_3$ -IE373-15 (Fig. 4a). The number of  $Ag$  nanoparticles was very limited; this is consistent with the low loading of silver (0.36 wt% as  $Ag$  metal) based on the X-ray absorbance. The chemical composition based on  $Ag$  K,  $Zn$  K, and  $Ga$  K-edge (Table 2a) suggested the formula  $Ag_{0.018}[Zn_3Ga_{0.91}(OH)_{7.8}](CO_3)_{0.45}\cdot7.1H_2O$  almost in consistent with ideal formula  $[Zn_3Ga(OH)_8](CO_3)_{0.5}\cdot mH_2O$  based on

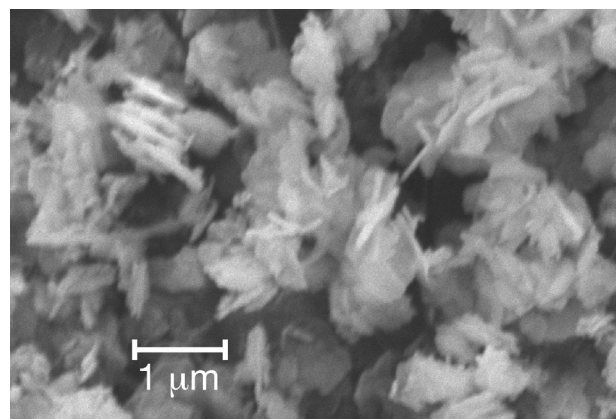


Fig. 3. SEM image for  $Ag/Zn_3Ga|CO_3$ -IE373-15.

Table 2

Chemical composition (wt%) of LDH composite samples based on X-ray absorption edge jump values.<sup>a</sup>

Entry	Sample	Ag	Au	Zn	Ga	(O, C, H)
(a)	$Ag/Zn_3Ga CO_3$ -IE373-15	0.36	–	35.7	11.5	(52.4)
(b)	$Au/Zn_3Ga CO_3$ -IE	–	2.2	–	–	–
(c)	$Ag/Zn_3Ga CO_3$ -reconst	10.2	–	–	–	–
(d)	$Au/Zn_3Ga CO_3$ -reconst	–	4.1	–	–	–

<sup>a</sup> XAFS spectra at  $Ag$  K,  $Zn$  K,  $Ga$  K, and  $Au$  L<sub>3</sub>-edges.

introduced amounts of precursors.  $Ag$  particles (2.2–8.0 nm, the mean size 3.6 nm) assembled with LDH by reconstruction method (Fig. 4b) and the loading of  $Ag$  was 10.2 wt% (Table 2c). The population of  $Ag$  nanoparticles were apparently higher than that for  $Ag/Zn_3Ga|CO_3$ -IE373-15 (Fig. 4a).

2.2–10.6 nm of  $Au$  particles (the mean size 3.2 nm) were observed in the HR-TEM image for  $Au/Zn_3Ga|CO_3$ -IE (Fig. 4c). The distribution was quite homogeneous. In the HR-TEM image for  $Au/Zn_3Ga|CO_3$ -reconst,  $Au$  nanoparticles (0.9–5.5 nm, the mean size 2.6 nm) during LDHs reconstruction process in the

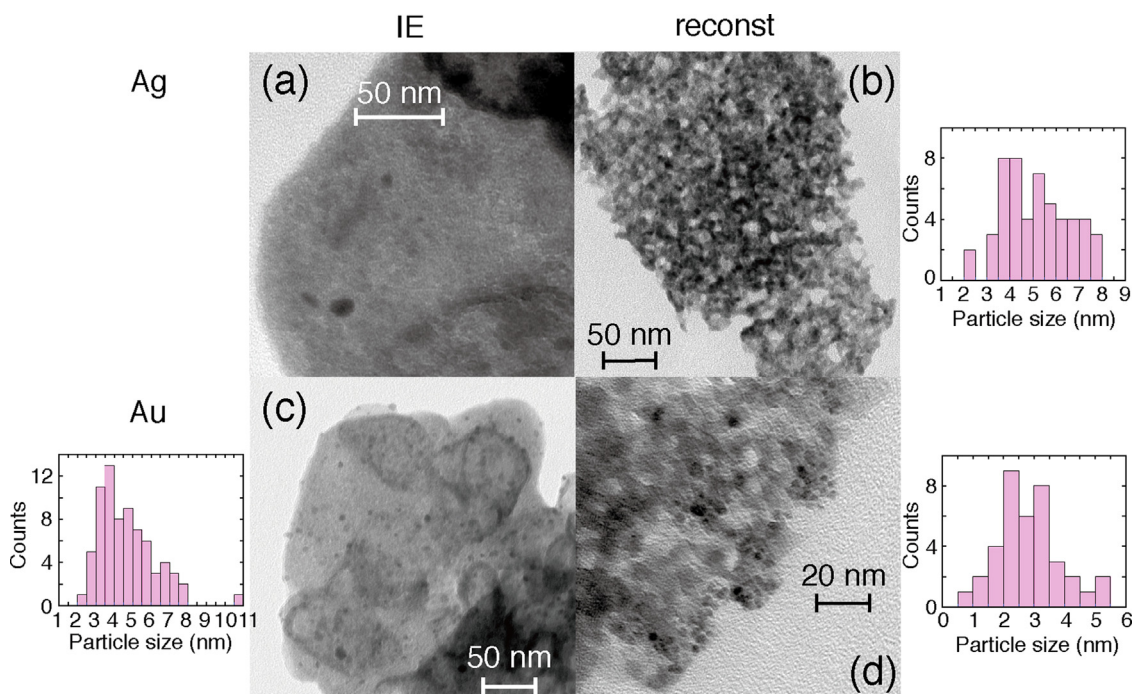
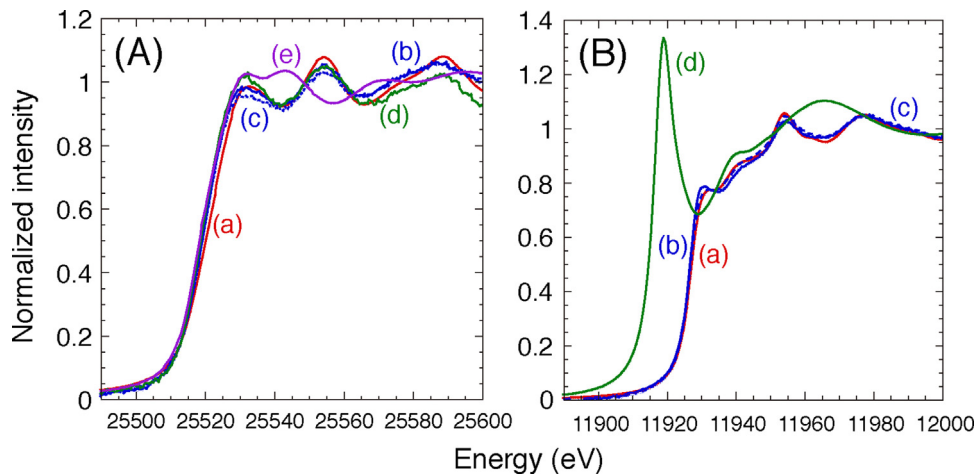


Fig. 4. TEM image for  $Ag/Zn_3Ga|CO_3$ -IE373-15 (a),  $Ag/Zn_3Ga|CO_3$ -reconst (b),  $Au/Zn_3Ga|CO_3$ -IE (c), and  $Au/Zn_3Ga|CO_3$ -reconst (d).



**Fig. 5.** (A) Normalized Ag K-edge XANES spectra for Ag metal foil (a), Ag/Zn<sub>3</sub>Ga|CO<sub>3</sub>-IE373-15 (b), sample b after photocatalytic test in CO<sub>2</sub> and H<sub>2</sub> for 5 h (c; dotted line), Ag/Zn<sub>3</sub>Ga|CO<sub>3</sub>-373-180 (d), and Ag<sub>2</sub>O (e). (B) Normalized Au L<sub>3</sub>-edge XANES spectra for Au metal foil (a), Au/Zn<sub>3</sub>Ga|CO<sub>3</sub>-IE (b), sample b after photocatalytic test in CO<sub>2</sub> and H<sub>2</sub> for 5 h (c; dotted line), and Au<sub>2</sub>O<sub>3</sub> + boron nitride (d).

presence of Au<sup>3+</sup> were clearly observed (Fig. 4d). The loading of Au was between 2.2 and 4.1 wt% for these samples (Table 2b and d). This evidenced that for Au/Zn<sub>3</sub>Ga|CO<sub>3</sub>-IE Au nanoparticles are distributed more homogeneous than that for Au/Zn<sub>3</sub>Ga|CO<sub>3</sub>-reconst, suggesting special interaction between the Au<sup>3+</sup> and oxides derived from Zn<sub>3</sub>Ga|CO<sub>3</sub> during the structural reconstruction process.

Ag K-edge X-ray absorption near-edge structure (XANES) spectra for Ag/Zn<sub>3</sub>Ga|CO<sub>3</sub>-IE373-15 and Ag/Zn<sub>3</sub>Ga|CO<sub>3</sub>-IE373-180 were depicted in Fig. 5A-b and d, respectively. The spectrum patterns in the XANES region for both LDH composite samples were quite similar to that for Ag metal (a) rather than Ag<sup>1/2</sup>O (e). Thus, Ag nanoparticles combined with LDH via the ion exchange method consisted of Ag<sup>0</sup> atoms. The metallic Ag<sup>0</sup> state of Ag/Zn<sub>3</sub>Ga|CO<sub>3</sub>-IE373-15 negligibly changed after the photocatalytic test in CO<sub>2</sub>

(2.3 kPa) and H<sub>2</sub> (21.7 kPa) for 5 h (Fig. 5A-c) in comparison to spectrum b for the as-synthesized sample. Similarly, metallic Au<sup>0</sup> state of fresh Au/Zn<sub>3</sub>Ga|CO<sub>3</sub>-IE remained after the photocatalytic test in CO<sub>2</sub> and H<sub>2</sub> for 5 h (Fig. 5B-b, c).

The  $k^3$ -weighted EXAFS function was depicted in Fig. 6a for Ag/Zn<sub>3</sub>Ga|CO<sub>3</sub>-IE373-15 (row 1) and Ag/Zn<sub>3</sub>Ga|CO<sub>3</sub>-IE373-180 (row 2). The associated Fourier transform is shown in the column b. The peaks at 0.27 nm (phase shift uncorrected) in the Fourier transform were nicely curve-fit by the parameters of Ag–Ag interatomic pair (Fig. 6c and d) and the fit results were listed in Table 3. The  $N$  value for Ag/Zn<sub>3</sub>Ga|CO<sub>3</sub>-IE373-15 was 7.6 (particle size ~1.6 nm), significantly smaller than  $N$  of 10.1 (particle size ~3.7 nm) for Ag/Zn<sub>3</sub>Ga|CO<sub>3</sub>-IE373-180 (Table 1A) [36], demonstrating the gradual growth of Ag nanoparticles during the reflux procedure at 373 K between 15 and 180 min.

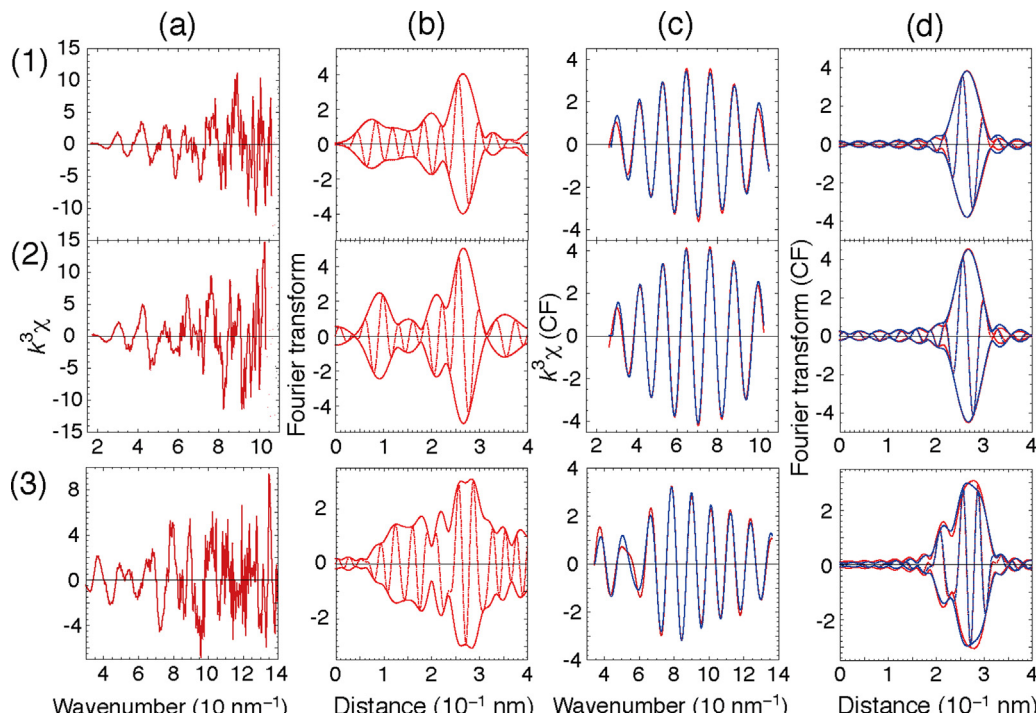


**Fig. 6.** Ag K-edge EXAFS for Ag/Zn<sub>3</sub>Ga|CO<sub>3</sub>-IE373-15 (1) and Ag/Zn<sub>3</sub>Ga|CO<sub>3</sub>-IE373-180 (2) and Au L<sub>3</sub>-edge EXAFS for Au/Zn<sub>3</sub>Ga|CO<sub>3</sub>-IE (3).  $k^3$ -weighted EXAFS oscillation (a), its associated Fourier transform (b), and best-fit results in  $k$ -space (c) and  $R$ -space (d).

**Table 3**

The curve-fit analysis results of Ag K and Au L<sub>3</sub>-edge EXAFS for Ag/Zn<sub>3</sub>Ga|CO<sub>3</sub>-IE and Au/Zn<sub>3</sub>Ga|CO<sub>3</sub>-IE samples.<sup>a</sup>

Sample	Ag–Ag or Au–Au		
	R (nm)	Goodness of fit	
	N	Δσ <sup>2</sup> (10 <sup>-5</sup> nm <sup>2</sup> )	
(a) Ag/Zn <sub>3</sub> Ga CO <sub>3</sub> -IE373-15	0.283 (±0.003) 7.6 (±0.7) 3.4 (±0.9)	7.0 × 10 <sup>3</sup>	
(b) Ag/Zn <sub>3</sub> Ga CO <sub>3</sub> -IE373-180	0.2895 (±0.0007) 10.1 (±0.3) 2.1 (±2.1)	2.9 × 10 <sup>3</sup>	
(c) Au/Zn <sub>3</sub> Ga CO <sub>3</sub> -IE	0.2878 (±0.003) 8.3 (±0.3) 1.0 (±0.2)	5.4 × 10 <sup>2</sup>	

<sup>a</sup> The values in parentheses are evaluated fit errors.

Although the instability of Ag and Au species in Ag/Zn<sub>3</sub>Ga|CO<sub>3</sub>-reconst and Au/Zn<sub>3</sub>Ga|CO<sub>3</sub>-reconst under the photocatalytic conditions was already suggested in UV-visible spectra (Fig. 1), tentative curve-fit analyses for fresh Ag/Zn<sub>3</sub>Ga|CO<sub>3</sub>-reconst and Au/Zn<sub>3</sub>Ga|CO<sub>3</sub>-reconst samples after photocatalytic tests in CO<sub>2</sub>+H<sub>2</sub> irradiated by UV-visible light for 5 h provided N value of 8.4 (particle size ~2.0 nm) for the Ag–Ag interatomic pair and N value of 7.7 (particle size ~1.7 nm) for the Au–Au interatomic pair (Table 1B). These mean particle sizes for Ag or Au were consistent with that obtained based on HR-TEM (3.6 and 2.6 nm, respectively; Table 1A). Furthermore, N(Au–Au) value of 8.3 (particle size ~1.9 nm) for fresh Au/Zn<sub>3</sub>Ga|CO<sub>3</sub>-IE was also consistent with mean particle size of 3.2 nm obtained based on HR-TEM (Table 1A). The detailed analyses for structure change of the Ag and Au sites during reconstruction step and photocatalytic tests are in progress [37].

### 3.2. Photocatalytic reduction of CO<sub>2</sub> using Ag/LDH and Au/LDH assemblies

The photocatalytic tests under CO<sub>2</sub>+H<sub>2</sub> and UV-visible light using Ag/Zn<sub>3</sub>Ga|CO<sub>3</sub>-IE373-15 produced mainly methanol (54 mol%) and minor CO as the reaction products (Table 4A-b and Fig. 7b). The total formation rate was 220 nmol h<sup>-1</sup> g<sub>cat</sub><sup>-1</sup>; thus improved by a factor of 1.69 times compared to that using Zn<sub>3</sub>Ga|CO<sub>3</sub> (130 nmol h<sup>-1</sup> g<sub>cat</sub><sup>-1</sup>; Table 4A-a) [10]. On the contrary, Ag/Zn<sub>3</sub>Ga|CO<sub>3</sub>-IE373-180 exhibited lower photocatalytic activity

giving rise only to CO (67 nmol h<sup>-1</sup> g<sub>cat</sub><sup>-1</sup>) and less than the detection limit of methanol (Table 4A-c and Fig. 7c). Based on the EXAFS curve fit analyses and XANES results, the increase of the mean diameter of Ag particles from ~1.6 nm to ~3.7 nm was demonstrated for the photocatalysts (Tables 1 and 3). The lower catalytic activity of Ag/Zn<sub>3</sub>Ga|CO<sub>3</sub>-IE373-180 might indicate a direct influence of the Ag nanoparticle size on the CO<sub>2</sub> photoreduction reactivity.

The photocatalytic performance of Ag/Zn<sub>3</sub>Ga|CO<sub>3</sub>-reconst was superior to that of Ag/Zn<sub>3</sub>Ga|CO<sub>3</sub>-IE373-180 (Fig. 7d), although decreased in comparison to that of Ag/Zn<sub>3</sub>Ga|CO<sub>3</sub>-IE373-15 or undoped Zn<sub>3</sub>Ga|CO<sub>3</sub> (Table 4A-a-d). The gray color of Ag/Zn<sub>3</sub>Ga|CO<sub>3</sub>-IE373-180 and Ag/Zn<sub>3</sub>Ga|CO<sub>3</sub>-reconst was maintained after the photocatalytic tests (Table 1B). Accordingly, a flat, wide absorption region in the visible light range was observed for these samples (Fig. 1d and e).

Major products distribution switched to CO (13–14 mol%) when Au/LDHs composites were tested as photocatalysts. Au/Zn<sub>3</sub>Ga|CO<sub>3</sub>-IE produced CO at a rate of 162 nmol h<sup>-1</sup> g<sub>cat</sub><sup>-1</sup> and the corresponded selectivity was equal to 86 mol% (Table 4A-e and Fig. 7e) in comparison to 46–68 mol% of CO using Zn<sub>3</sub>Ga|CO<sub>3</sub> and Zn<sub>3</sub>Ga|CO<sub>3</sub> composites with Ag nanoparticles (Table 4A-a-d). The CO formation rate was even higher using Au/Zn<sub>3</sub>Ga|CO<sub>3</sub>-reconst (201 nmol h<sup>-1</sup> g<sub>cat</sub><sup>-1</sup>; Fig. 7f) than that using Au/Zn<sub>3</sub>Ga|CO<sub>3</sub>-IE (Table 4A-e, f). The Au/Zn<sub>3</sub>Ga|CO<sub>3</sub>-reconst photocatalyst exhibited the best performance on the total formation rate. Total product formation rate was 231 nmol h<sup>-1</sup> g<sub>cat</sub><sup>-1</sup>, improved by a factor of 1.78 times compared to that using Zn<sub>3</sub>Ga|CO<sub>3</sub> (Table 4f).

The stoichiometry of formed molar amount (n) of methanol, CO, and water following Eqs (1) and (2) ( $n_{\text{methanol}} + n_{\text{CO}} = n_{\text{water}}$ ) was consistent using Ag/Zn<sub>3</sub>Ga|CO<sub>3</sub>-IE-373-15, Ag/Zn<sub>3</sub>Ga|CO<sub>3</sub>-reconst, and Au/Zn<sub>3</sub>Ga|CO<sub>3</sub>-reconst (Fig. 7b, d, f). Further, 74% excessive water was obtained on Ag/Zn<sub>3</sub>Ga|CO<sub>3</sub>-IE373-180 (Fig. 7c), probably due to structural water desorbed from the interlayer space of Zn<sub>3</sub>Ga|CO<sub>3</sub> LDH. On the contrary, the formed water was 48 mol% of the total amount of methanol and CO formed when Au/Zn<sub>3</sub>Ga|CO<sub>3</sub>-IE were tested as a photocatalyst (Fig. 7e). This could be the consequence that part of the formed water might be adsorbed on the photocatalyst.

To confirm the role of the SPR effect and/or electron trap sites of Ag or Au nanoparticles, the photoreduction of CO<sub>2</sub> by H<sub>2</sub> under visible light irradiation ( $\lambda > 420$  nm) were also performed (Fig. 7b' and Table 4B) and the results were compared to that obtained when UV-visible light were used for irradiation (see Table 4A).

Under visible light only, Zn<sub>3</sub>Ga|CO<sub>3</sub> did not produce any products above the detection limit of GC. On the contrary, Ag/Zn<sub>3</sub>Ga|CO<sub>3</sub>-IE373-15 exhibited 31 and 86% of methanol and CO formation rates, respectively, compared to the corresponding rates

**Table 4**

Photocatalytic rates of CO<sub>2</sub> reduction with H<sub>2</sub> using the nanoparticles/LDH catalysts.<sup>a</sup>

Entry	Photocatalyst	Formation rate (nmol h <sup>-1</sup> g <sub>cat</sub> <sup>-1</sup> )			Selectivity to CH <sub>3</sub> OH (mol%)	Reference
		CH <sub>3</sub> OH	CO	Σ		
<i>(A) Irradiated by UV-visible light</i>						
a	Zn <sub>3</sub> Ga CO <sub>3</sub>	51	80	130	39	[10]
b	Ag/Zn <sub>3</sub> Ga CO <sub>3</sub> -IE373-15	118	102	220	54	This work
c	Ag/Zn <sub>3</sub> Ga CO <sub>3</sub> -IE373-180	<12	67	67	<15	This work
d	Ag/Zn <sub>3</sub> Ga CO <sub>3</sub> -reconst <sup>b</sup>	30	64	94	32	This work
e	Au/Zn <sub>3</sub> Ga CO <sub>3</sub> -IE	26	162	187	14	this work
f	Au/Zn <sub>3</sub> Ga CO <sub>3</sub> -reconst <sup>b</sup>	30	201	231	13	This work
<i>(B) Irradiated by visible light (<math>\lambda &gt; 420</math> nm)</i>						
a	Zn <sub>3</sub> Ga CO <sub>3</sub>	<4	<8	<12	<33	[10]
b	Ag/Zn <sub>3</sub> Ga CO <sub>3</sub> -IE373-15	36	88	124	29	This work
e	Au/Zn <sub>3</sub> Ga CO <sub>3</sub> -IE	<4	<8	<12	<33	This work
f	Au/Zn <sub>3</sub> Ga CO <sub>3</sub> -reconst <sup>b</sup>	<4	<8	<12	<33	This work

<sup>a</sup> In CO<sub>2</sub>(2.3 kPa)+H<sub>2</sub>(21.7 kPa). The catalyst amount was 100 mg. Values in parentheses are evaluated fit errors.

<sup>b</sup> Preheated at 373 K for 30 min.

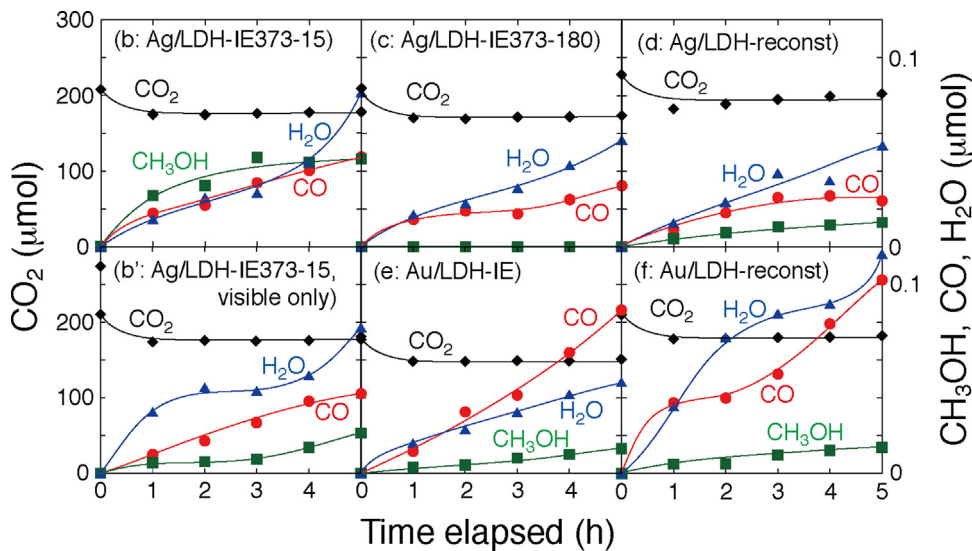


**Fig. 7.** Time course of photocatalytic tests under  $\text{CO}_2$  (2.3 kPa) and  $\text{H}_2$  (21.7 kPa) using UV-visible light and  $\text{Ag}/\text{Zn}_3\text{Ga}|\text{CO}_3$ -IE373-15 (b),  $\text{Ag}/\text{Zn}_3\text{Ga}|\text{CO}_3$ -IE373-180 (c),  $\text{Ag}/\text{Zn}_3\text{Ga}|\text{CO}_3$ -reconst (d),  $\text{Au}/\text{Zn}_3\text{Ga}|\text{CO}_3$ -IE (e), and  $\text{Au}/\text{Zn}_3\text{Ga}|\text{CO}_3$ -reconst (f). Time course of comparison tests under  $\text{CO}_2$  (2.3 kPa) and  $\text{H}_2$  (21.7 kPa) using visible light ( $\lambda > 420 \text{ nm}$ ) and  $\text{Ag}/\text{Zn}_3\text{Ga}|\text{CO}_3$ -IE373-15 (b').  $\text{CO}_2$  (♦; diamond),  $\text{H}_2\text{O}$  (▲; triangle),  $\text{CH}_3\text{OH}$  (■; square), and  $\text{CO}$  (●; circle).

under UV-visible light (Tables 4A-b and 3B-b). The stoichiometry following Eqs. (1) and (2) was preserved when irradiation by visible light was used (Fig. 7b'). This might suggest that the LDHs is able to utilize UV light for the photocatalysis while Ag nanoparticles are able to promote the  $\text{CO}_2$  photoreduction by utilizing the SPR response. It is worthy to note that Au based catalysts were not active when visible light ( $\lambda > 420 \text{ nm}$ ) was used for irradiation (Table 4B-e, f).

## 4. Discussion

### 4.1. Structure of Ag/LDH and Au/LDH catalysts

Regular layered structures with the interlattice distance between 0.752 and 0.754 nm were confirmed for  $\text{Zn}_3\text{Ga}|\text{CO}_3$  and all the assemblies of  $\text{Zn}_3\text{Ga}|\text{CO}_3$  LDH with Ag or Au nanoparticles tested in this study (Table 1). The interlattice distance corresponds to the LDH containing carbonate and water molecules in the interlayers [10] revealing that Ag and Au nanoparticles might be located only on the surface of the platelets of  $\text{Zn}_3\text{Ga}|\text{CO}_3$  (that are defined by sizes between 200 and 700 nm and the thickness between 20 and 50 nm, see Fig. 3). Ag nanoparticles of 5.4–27 nm were observed by the HR-TEM for  $\text{Ag}/\text{Zn}_3\text{Ga}|\text{CO}_3$ -IE373-15 (Fig. 4a). The loading of Ag nanoparticles was low (0.36 wt% as Ag metal, Table 2a), and the  $N$  value obtained by the EXAFS curve fit analysis for the sample was 7.6 (Table 3a) suggesting a mean particle size defined by a mean diameter of ~1.6 nm (Table 1A). This discrepancy of particle size might be the consequence to the limited number of Ag nanoparticles, but also the difficulty to observe very small Ag nanoparticles in our HR-TEM analysis.

Au nanoparticles with a diameter inside the range of [0.9–5.5] nm were observed in the HR-TEM for  $\text{Au}/\text{Zn}_3\text{Ga}|\text{CO}_3$ -reconst (Fig. 4d). Hence for this photocatalyst, the mean diameter of Au nanoparticles is equal to 2.6 nm (see Table 1A). This result is consistent with the SPR peak situated at 555 nm (Fig. 1A) that, in agreement with the previous studies correspond to Au nanoparticles of 2–3 nm [14].

The mean particle sizes of Ag or Au for  $\text{Ag}/\text{Zn}_3\text{Ga}|\text{CO}_3$ -reconst (3.6 nm),  $\text{Au}/\text{Zn}_3\text{Ga}|\text{CO}_3$ -IE (3.2 nm), and  $\text{Au}/\text{Zn}_3\text{Ga}|\text{CO}_3$ -reconst (2.6 nm) obtained based on HR-TEM (Table 1A and Fig. 4) were

in consistent with values (2.0, 1.9, and 1.7, respectively) based on EXAFS (Tables 1A, B and 3 and Fig. 6).

### 4.2. Roles in $\text{CO}_2$ photoreduction of the photocatalyst components: LDH and nanoparticles of Ag/Au

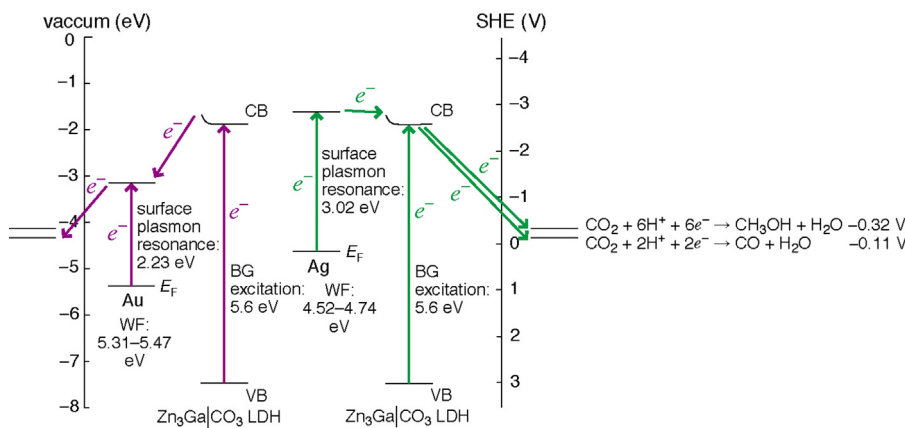
$\text{Zn}_3\text{Ga}|\text{CO}_3$  photocatalyst photoreduced  $\text{CO}_2$  into CO and methanol using  $\text{H}_2$  (Table 4A-a) [10]. The formation rates of CO and methanol both increased for  $\text{Ag}/\text{Zn}_3\text{Ga}|\text{CO}_3$ -IE373-15. In fact, the total formation rate of  $\text{Ag}/\text{Zn}_3\text{Ga}|\text{CO}_3$ -IE373-15 increased by a factor of 1.69 times compared to that of  $\text{Zn}_3\text{Ga}|\text{CO}_3$ . The change of methanol selectivity from 39 to 54 mol% was enough moderate (Table 4A-b).

For Au based catalysts, the total formation rates of CO and methanol using  $\text{Au}/\text{Zn}_3\text{Ga}|\text{CO}_3$ -IE and  $\text{Au}/\text{Zn}_3\text{Ga}|\text{CO}_3$ -reconst increased by 1.44 and 1.78 times, respectively, in comparison to  $\text{Zn}_3\text{Ga}|\text{CO}_3$ . Hence, the selectivity to CO increased from 61 mol% for  $\text{Zn}_3\text{Ga}|\text{CO}_3$  to 86–87 mol% (Table 4A-e, f) for  $\text{Au}/\text{Zn}_3\text{Ga}|\text{CO}_3$ , suggesting different promoting mechanisms/sites.

The energy diagram and proposed electron flows during the photocatalytic process are illustrated in Scheme 1 considering the work function (WF) of Ag (4.52–4.74 eV) and Au (5.31–5.47 eV) [38,39], wavelength of SPR peak top (411 nm for  $\text{Ag}/\text{Zn}_3\text{Ga}|\text{CO}_3$ -373-15, 555 nm for  $\text{Au}/\text{Zn}_3\text{Ga}|\text{CO}_3$ -reconst; Fig. 1A and Table 1), bandgap values of the  $\text{Zn}_3\text{Ga}|\text{CO}_3$  LDH (Table 1A), and the reaction potential values for  $\text{CO}_2$  reduction to CO (−0.11 V versus SHE) and for  $\text{CO}_2$  reduction to methanol (−0.32 V versus SHE) [10].

Based on the above results, we assume that the photoreduction of  $\text{CO}_2$  by  $\text{H}_2$  (Table 4), under irradiation with UV and visible light might induce both bandgap excitation of  $\text{Zn}_3\text{Ga}|\text{CO}_3$  (5.6 eV) and the surface plasmon excitation (2.23–3.02 eV), respectively. Due to the difference in the values of WF and SPR energy for Au (3.1–3.2 eV) and Ag (1.5–1.7 eV), excited electrons at conduction band (CB) for  $\text{Zn}_3\text{Ga}|\text{CO}_3$  might be transferred to Au whereas the SPR-excited electrons at Ag nanoparticles might migrate to  $\text{Zn}_3\text{Ga}|\text{CO}_3$  LDH (see Scheme 1).

The higher selectivity to CO using  $\text{Au}/\text{Zn}_3\text{Ga}|\text{CO}_3$ -reconst and  $\text{Au}/\text{Zn}_3\text{Ga}|\text{CO}_3$ -IE (86–87 mol%) might suggest that the contribution of Au sites via the electron transfer derived from the band gap excitation of the  $\text{Zn}_3\text{Ga}|\text{CO}_3$  support. On the contrary, for  $\text{Zn}_3\text{Ga}|\text{CO}_3$  (CO selectivity: 61 mol%),  $\text{Ag}/\text{Zn}_3\text{Ga}|\text{CO}_3$ -IE373-15, and



**Scheme 1.** The energy diagram and proposed electron flows in Ag/Zn<sub>3</sub>Ga|CO<sub>3</sub>-IE373-15 (right) and Au/Zn<sub>3</sub>Ga|CO<sub>3</sub>-reconst (left) during photocatalytic reduction of CO<sub>2</sub>.

Ag/Zn<sub>3</sub>Ga|CO<sub>3</sub>-reconst (46–68 mol%), Ag nanoparticles on the LDH surface might be involved as major electron-donating sites during CO<sub>2</sub> photoreduction. This agrees well to the previous reported results for Au nanoparticles deposited on glass (to form methane, formaldehyde, ethane, and methanol) showing the direct contribution of Au in CO<sub>2</sub> photoreduction [19]. It should be noted that excited electrons due to SPR of nanosized Ag or Au were not always inserted to wide-E<sub>g</sub> LDH Zn<sub>3</sub>Ga|CO<sub>3</sub> (5.6 eV), in comparison to the insertion from Au [17–19] and Ag nanoparticles [17] to TiO<sub>2</sub> (E<sub>g</sub>: 3.0–3.2 eV).

Therefore, results points out that Ag/Zn<sub>3</sub>Ga|CO<sub>3</sub>-IE373-15 catalyzed the photoreduction of CO<sub>2</sub> in a similar way to Zn<sub>3</sub>Ga|CO<sub>3</sub>, boosted by Ag sensitization by the electron transfer from the nanoparticles of Ag to LDH either (i) by the hot electron transfer, (ii) thermally excited electron transfer, or (iii) plasmonic resonant energy transfer [17–20]. This dependence on wavelength of irradiated light was similar to the behavior of photooxidation of methanol/ethanol using Au/TiO<sub>2</sub> [18].

Furthermore, the assemblies of the LDH with Au nanoparticles were inert when irradiated by visible light ( $\lambda > 420$  nm) (Table 4B-e, f). The electrons created by SPR of Au are not able to photoreduce CO<sub>2</sub> by visible light, whereas E<sub>g</sub>-excited electrons in LDH by UV light was trapped in Au and then transferred to CO<sub>2</sub>-derived species. As the potential of excited electrons at Au is lower (more positive) than that of excited electrons at the CB of Zn<sub>3</sub>Ga|CO<sub>3</sub>, energetically favorable CO formation would have a priority rather than methanol formation in the presence of UV light (Scheme 1).

## 5. Conclusions

The present results illustrate the potential of the plasmonic nanostructured assemblies of Au/Zn<sub>3</sub>Ga(OH)<sub>8</sub>]<sub>2</sub>CO<sub>3</sub>·mH<sub>2</sub>O and Ag/Zn<sub>3</sub>Ga(OH)<sub>8</sub>]<sub>2</sub>CO<sub>3</sub>·mH<sub>2</sub>O as photocatalysts for CO<sub>2</sub> reduction by H<sub>2</sub> using both UV and visible light. The CO<sub>2</sub> photoreduction rate using Ag/Zn<sub>3</sub>Ga|CO<sub>3</sub>-IE catalyst was higher (220 nmol h<sup>-1</sup> g<sub>cat</sub><sup>-1</sup>) by a factor of 1.69 in comparison to that of Zn<sub>3</sub>Ga|CO<sub>3</sub>. Under visible light irradiation, the photoreduction rate of Ag/Zn<sub>3</sub>Ga|CO<sub>3</sub>-IE decreased to 56% of corresponding rate under irradiation with UV-visible light. Moreover, Au/Zn<sub>3</sub>Ga|CO<sub>3</sub>-reconst irradiated by UV-visible light showed the best catalytic performances (231 nmol h<sup>-1</sup> g<sub>cat</sub><sup>-1</sup>), although these catalysts were CO selective (87 mol%). All Au/Zn<sub>3</sub>Ga|CO<sub>3</sub> were found to be inert for CO<sub>2</sub> photoreduction by H<sub>2</sub> when irradiated by visible light ( $\lambda > 420$  nm). We present evidence that Ag nanoparticles might assist the metal/LDH assemblies' photoreduction activity by the electron injection due to the SPR effect while the Au nanoparticles might act as electron trap excited in the LDH matrix irradiated by UV light. The optimized

design of the plasmonic nanoparticles-LDH self-assemblies can open the way for further development of novel promising catalysts for CO<sub>2</sub> photoreduction.

## Acknowledgments

The authors are grateful for the financial supports from the Grant-in-Aid for Scientific Research C (26410204, 22550117) from Japan Science Promotion Agency and from the Romanian National Authority for Scientific Research, CNCS-UEFISCDI (PN-II-IDEEI-PCE-75/2013). X-ray absorption experiments were conducted under the approval of the Photon Factory Proposal Review Committee (2014G631, 2011G033).

## References

- [1] A. Corma, H. García, J. Catal. 308 (2013) 168–175.
- [2] Y. Izumi, Coord. Chem. Rev. 257 (2013) 171–186.
- [3] S.C. Roy, O.K. Varghese, M. Paulose, C.A. Grimes, ACS Nano 4 (2010) 1259–1278.
- [4] D.B. Ingram, S. Linic, J. Am. Chem. Soc. 133 (2011) 5202–5205.
- [5] F. Cavaní, F. Trifirò, A. Vaccari, Catal. Today 11 (1991) 173–301.
- [6] C. Gomes Silva, Y. Bouizi, V. Fornés, H. García, J. Am. Chem. Soc. 131 (2009) 13833–13839.
- [7] Z. Yong, A.E. Rodrigues, Energy Convers. Manag. 43 (2002) 1865–1876.
- [8] M. Morikawa, N. Ahmed, Y. Yoshida, Y. Izumi, Appl. Catal. B144 (2014) 561–569.
- [9] N. Ahmed, M. Morikawa, Y. Izumi, Catal. Today 185 (2012) 263–269.
- [10] N. Ahmed, Y. Shibata, T. Taniguchi, Y. Izumi, J. Catal. 279 (2011) 123–135.
- [11] K. Teramura, S. Iguchi, Y. Mizuno, T. Shishido, T. Tanaka, Angew. Chem. Int. Ed. 51 (2012) 8008–8011.
- [12] M. Morikawa, Y. Ogura, N. Ahmed, S. Kawamura, G. Mikami, S. Okamoto, Y. Izumi, Catal. Sci. Technol. 4 (2014) 1644–1651.
- [13] R.E. Blankenship, D.M. Tiede, J. Barber, G.W. Brudvig, G. Fleming, M. Ghirardi, M.R. Gunner, W. Junge, D.M. Kramer, A. Melis, T.A. Moore, C.C. Moser, D.G. Nocera, A.J. Nozik, D.R. Ort, M.W. Parson, R.C. Prince, R.T. Sayre, Science 332 (2011) 805–809.
- [14] [http://www.cytodiagnostics.com/silver\\_nanoparticle\\_properties.php](http://www.cytodiagnostics.com/silver_nanoparticle_properties.php)
- [15] [http://www.cytodiagnostics.com/gold\\_nanoparticle\\_properties.php](http://www.cytodiagnostics.com/gold_nanoparticle_properties.php)
- [16] O. Nicoletti, F. de la Pena, R.K. Leary, D.J. Holland, C. Ducati, P.A. Midgley, Nature 502 (2013) 80–84.
- [17] C. Clavero, Nat. Photonics 8 (2014) 95–103.
- [18] Y. Tian, T. Tatsuma, J. Am. Chem. Soc. 127 (2005) 7632–7637.
- [19] W. Hou, W.H. Hung, P. Pavaskar, A. Goepert, M. Aykol, S.B. Cronin, ACS Catal. 1 (2011) 929–936.
- [20] S.K. Cushing, J. Li, F. Meng, T.R. Senty, S. Suri, M. Zhi, M. Li, A.D. Bristow, N. Wu, J. Am. Chem. Soc. 134 (2012) 15033–15041.
- [21] G. Carja, Y. Kameshima, A. Nakajima, C. Dranca, K. Okada, Int. J. Antimicrob. Agent 34 (2009) 534–539.
- [22] G. Carja, M. Birsanu, K. Okada, H. García, J. Mol. Mater. Chem. A 1 (2013) 9092–9098.
- [23] C. Chen, P. Gunawan, X.W. Lou, R. Xu, Adv. Funct. Mater. 22 (2012) 780–787.
- [24] L. Wang, J. Zhang, X. Meng, D. Zheng, F.S. Xiao, Catal. Today 175 (2011) 404–410.
- [25] F. Wooten, Optical Properties of Solids, Academic Press, New York, USA, 1972, pp. 142.
- [26] J.A. Bearden, Rev. Mod. Phys. 39 (1967) 78–124.
- [27] M. Vaarkamp, H. Linders, D. Koningsberger, XDAP version 2.2.7, XAFS Services International, Woudenberg, The Netherlands, 2006.

- [28] Y. Izumi, T. Itoi, S. Peng, K. Oka, Y. Shibata, *J. Phys. Chem. C* 113 (2009) 6706–6718.
- [29] L.G. Liu, W.A. Bassett, *J. Appl. Phys.* 44 (1973) 1475–1479.
- [30] C. Petitjean, D. Horwat, J.F. Pierson, *J. Phys. D* 42 (2009) 025304.
- [31] S. Fujii, U. Akiba, M. Fujihira, *J. Am. Chem. Soc.* 124 (2002) 13629–13635.
- [32] X. Liu, G. Qiu, Y. Zhao, N. Zhang, R. Yi, *J. Alloys Compd.* 439 (2007) 275–278.
- [33] Y. Yoshida, Y. Mitani, T. Itoi, Y. Izumi, *J. Catal.* 287 (2012) 190–202.
- [34] A.E. Rakhshani, A. Bumajdad, J. Kokaj, S. Thomas, *Appl. Phys. A* 97 (2009) 759–764.
- [35] K. Kusaba, T. Yagi, J. Yamaura, H. Gotou, T. Kikegawa, *J. Phys. Conf. Ser.* 215 (2010) 012001.
- [36] B.J. Kip, F.B.M. Duivenvoorden, D.C. Koningsberger, R. Prins, *J. Catal.* 105 (1987) 26–38.
- [37] S. Kawamura, G., Carja, Y. Izumi, in preparation.
- [38] R.C. Weast, *CRC Handbook of Chemistry and Physics*, vol. 82, CRC Press, Boca Raton, USA, 2001, pp. 12–130.
- [39] Y. Ogura, S. Okamoto, T. Itoi, Y. Fujishima, Y. Yoshida, Y. Izumi, *Chem. Commun.* 50 (2014) 3067–3070.